J. Plasma Phys. (2021), *vol*. 87, 905870105
Published by Cambridge University Press
doi:10.1017/S0022377820001579

On the thermal effects on radio waves propagating in the pulsar magnetosphere

A. G. Mikhaylenko[1], **V. S. Beskin**[1,2],† **and Ya. N. Istomin**[1,2]

[1]Moscow Institute of Physics and Technology, Institutsky per. 9, Dolgoprudny, 147000, Russia

[2]P.N.Lebedev Physical Institute, Leninsky prosp. 53, Moscow, 119991, Russia

(Received 11 December 2019; revised 3 December 2020; accepted 4 December 2020)

Thermal effects on the properties of four electromagnetic waves propagating in the pulsar magnetosphere are analysed. It is shown that thermal effects change only quantitatively the dispersion properties of superluminal ordinary O-mode freely escaping the pulsar magnetosphere; whereas properties of the extraordinary X-mode remain unchanged. The research shows that for two subluminal waves propagating along magnetic field lines thermal effects result in essential absorption. However, this attenuation occurs at considerable distances from the neutron star, and there is no doubt of their existence.

Key words: astrophysical plasmas

1. Introduction

Unfortunately, at present the theory of pulsar radio emission is far from the mainstream of modern astrophysics. This problem was not solved in the 1970–80s, and we have no consistent theory up to now (Manchester & Taylor 1977; Michel 1991; Mestel 1999; Lorimer & Kramer 2012; Lyne & Graham-Smith 2012). Moreover, the discussion for some key points has been actually frozen. For this reason, the new generation of scientists is not familiar with state-of-the-art research done in this field (Goldreich & Keeley 1971; Blandford 1975; Ginzburg & Zheleznyakov 1975; Suvorov & Chugunov 1975; Blandford & Scharlemann 1976; Benford & Buschauer 1977; Hardee & Rose 1978; Lominadze & Mikhailovskii 1979; Lominadze, Mikhailovskii & Sagdeev 1979; Asseo, Pellat & Sol 1983; Lominadze, Machabeli & Usov 1983; Larroche & Pellat 1987; Usov 1987; Melrose & Gedalin 1999). In recent years, research has been conducted only in the theory of wave propagation (Barnard & Arons 1986; Blaskiewicz, Cordes & Wasserman 1991; Han *et al.* 1998; Lyubarskii & Petrova 1998, 2000; Petrova 2001; Dyks 2008; Andrianov & Beskin 2010; Wang, Lai & Han 2010; Beskin & Philippov 2012; Wang, Wang & Han 2014, 2015; Yuen & Melrose 2014; Hakobyan, Beskin & Philippov 2017), but not into the mechanism of radio emission itself.

So, to date, there have been several dozen models of pulsar radio emission of varying degrees of elaboration (see, e.g. Volokitin, Krasnoselskh & Machabeli 1985; Beskin, Gurevich & Istomin 1988; Ursov & Usov 1988; Asseo, Pelletier & Sol 1990; Kazbegi, Machabeli & Melikidze 1991; Weatherall 1994; Gedalin, Gruman & Melrose 1999;

† Email address for correspondence: beskin@lpi.ru

Lyutikov, Blandford & Machabeli 1999; Philippov *et al.* 2019; Philippov, Timokhin & Spitkovsky 2020), which relate little to each other. For this reason, we do not intend to carry out their detailed analysis. We consider only one controversial issue, which, apparently, finds its solution. The point is that in the theory of pulsar radio emission there was not agreement with such a seemingly obvious question as the number of radio waves propagating outwards from a neutron star. Most authors insisted that there are only three modes (Barnard & Arons 1986; Lyutikov 1999; Usov 2006; Lyubarsky 2008), i.e. two transverse and one plasma wave, whereas according to Beskin *et al.* (1988) and Beskin, Gurevich & Istomin (1993) (see also Lyne & Graham-Smith 2012) there are four waves. And the works, claiming that the number of modes is only three, appeared until very recently (Melrose & Rafat 2017).

Actually, this was the result of misunderstanding, since Beskin *et al.* (1988) did not discuss the 'fourth mode', but another branch of the plasma mode. Indeed, adopting the convention in which the wave modes are defined in the plasma rest frame, we conclude that there are only three wave modes, i.e. two transverse and one plasma mode. But another convention is to interpret as an additional mode any positive-frequency, forward-propagating solution in the pulsar rest frame which arises by a Lorentz transforming of a negative frequency or backward-propagating solution in a plasma reference frame. Below we use the second convention, which, after the work by Rafat, Melrose & Mastrano (2019*b*) and especially after Melrose, Rafat & Mastrano 2020 (see their text after (19)), should no longer raise objections.

On the other hand, Rafat *et al.* (2019*b*) posed another important problem related to this issue. The point is that in the work by Beskin *et al.* (1988), it was assumed that the energy spread of outflowing particles is small in comparison with their mean energy. The same approximation was later used by Lyubarskii & Petrova (1998, 2000). But according to numerous studies on the generation of a secondary electron–positron plasma in the polar regions of a neutron star (Daugherty & Harding 1982; Gurevich & Istomin 1985; Arendt & Eilek 2002; Medin & Lai 2010; Timokhin 2010; Timokhin & Harding 2015), in the rest system of the plasma, the temperature is to be of the order of the rest mass of the particles. As a result, the dispersion properties of waves propagating in the pulsar magnetosphere can change significantly. The question of how thermal effects (i.e. the presence of a significant spread of particles in energies comparable to the mean energy of the plasma motion) affect the dispersion properties of radio waves in the radio pulsar magnetosphere is the main topic of this work.

Thus, in this paper we analyse how the thermal effects can change the dispersion properties of all the four waves propagating outwards in the pulsar magnetosphere. In particular, we show that for superluminal O-mode the hydrodynamical approximation remains good enough even for high temperature, $T \sim 1$ MeV. As for two subluminal modes, for them, the kinetic effects result in more effective damping. Notably, these modes cannot escape the pulsar magnetosphere as at a large distance from the neutron star they propagate along magnetic field lines.

We emphasize once again that we did not set ourselves the task of analysing the various mechanisms of radio emission. Our task was to elucidate the dispersion properties of waves whose frequencies belong to the radio range (in connection with the problem of their propagation in the pulsar magnetosphere). Therefore the results of our research can be used to study the propagation of waves emitted by any radiation mechanism. For this reason, below we will only briefly discuss the effects occurring in the radiation region. We recall that observations unambiguously confirm the presence of two orthogonal modes in the radio emission of pulsars.

The paper is structured as follows. Section 2 provides a detailed description of a problem emphasizing that our main goal is to study the properties of waves generated in the inner regions of the pulsar magnetosphere. General description of waves propagating in superstrong magnetic fields is beyond the scope of our consideration. Section 3 describes superluminal wave connected with ordinary O-mode freely escaping from the magnetosphere. We show that thermal effects do not drastically affect its trajectory. Further, §§ 4 and 5 show how thermal effects result in more effective damping of two subluminal waves propagating along magnetic field lines. Section 6 provides an example of another energy distribution function and shows how the distribution function itself affects the waves properties. Finally, we summarize the results of our research.

2. Description of the problem

To begin with, it is necessary to clearly formulate the task which will be discussed later in this section, as well as the area of the considered parameters. This, as we shall see, removes a significant number of contentious issues.

First of all, we do not consider the general dispersion properties of electromagnetic waves but limit ourselves only to frequencies which fall in the observable radio frequency band 100 MHz–10 GHz. This is one of the main differences from the works of Rafat, Melrose & Mastrano (2019*a*) and Rafat *et al.* (2019*b*), who analysed the dispersion properties of subluminal waves for arbitrary Lorentz factor of the wave phase velocity γ_ϕ. The authors showed that there is a sufficiently large range of values of γ_ϕ, in which there is a good agreement with the results of Beskin *et al.* (1988). As will be shown later in this section, it is this region that corresponds to the observed radio frequencies.

Second, we consider the standard parameters of plasma in the vicinity of the neutron star, where the generation of radio emission is supposed to occur. Assuming that the magnetic field on the surface of a neutron star is $B_0 = 10^{12}$ G, we find that $B = 10^9$–10^{12} G for distances r up to 10 neutron star radii R. For such a large magnetic field, the gyrofrequency $\omega_B = eB/m_e c$ is several orders of magnitude larger than the radio frequency ω. For this reason, in what follows we neglect all the small terms $\sim \omega/\omega_B$. In other words, we consider the case of infinite external magnetic field $B \to \infty$. This implies that only the parallel component of the wave electric field can interact with particles.

Here, however, one important remark should be made. In a strong magnetic field, when for cold plasma the dielectric permittivity tensor ε_{ij} has the form (see, e.g. Suvorov & Chugunov 1975; Hardee & Rose 1978)

$$\varepsilon_{ij} = \begin{bmatrix} 1+\dfrac{\omega_{\rm pe}^2\gamma\tilde{\omega}^2}{\omega^2(\omega_B^2-\gamma^2\tilde{\omega}^2)}, & \mathrm{i}\dfrac{\omega_{\rm pe}^2\omega_B\tilde{\omega}}{\omega^2(\omega_B^2-\gamma^2\tilde{\omega}^2)}, & \dfrac{\omega_{\rm pe}^2\gamma k_x v\tilde{\omega}}{\omega^2(\omega_B^2-\gamma^2\tilde{\omega}^2)} \\ -\mathrm{i}\dfrac{\omega_{\rm pe}^2\omega_B\tilde{\omega}}{\omega^2(\omega_B^2-\gamma^2\tilde{\omega}^2)}, & 1+\dfrac{\omega_{\rm pe}^2\gamma\tilde{\omega}^2}{\omega^2(\omega_B^2-\gamma^2\tilde{\omega}^2)}, & -\mathrm{i}\dfrac{\omega_{\rm pe}^2\omega_B k_x v}{\omega^2(\omega_B^2-\gamma^2\tilde{\omega}^2)} \\ \dfrac{\omega_{\rm pe}^2\gamma k_x v\tilde{\omega}}{\omega^2(\omega_B^2-\gamma^2\tilde{\omega}^2)}, & \mathrm{i}\dfrac{\omega_{\rm pe}^2\omega_B k_x v}{\omega^2(\omega_B^2-\gamma^2\tilde{\omega}^2)}, & 1-\dfrac{\omega_{\rm pe}^2}{\gamma^3\tilde{\omega}^2}+\dfrac{\omega_{\rm pe}^2\gamma k_x^2 v^2}{\omega^2(\omega_B^2-\gamma^2\tilde{\omega}^2)} \end{bmatrix}, \tag{2.1}$$

where $\tilde{\omega} = \omega - \boldsymbol{kv}$ and hydrodynamical velocity $\boldsymbol{v} \parallel \boldsymbol{B}$, the transition from quasi-longitudinal to quasi-transverse approximation occurs at small enough angles θ_b between the wavevector $\boldsymbol{k}$ and external magnetic field $\boldsymbol{B}$. Moreover, for $\theta_b \approx \theta_{\rm cr} = \omega_{\rm pe}/\omega_B$ (see, e.g. Zheleznyakov 1970) mode crossing takes place; therefore, additional thermal effects should be expected for such small angles.

However, within physical parameters under consideration, this intersection occurs at the angles θ_b much smaller than the opening angle of the radiation pattern of the emitting particles $\theta_{\rm rad} \sim 1/\gamma$ ($\theta_{\rm cr}/\theta_{\rm rad} \ll 1$, see below). In addition, such a mode crossing takes place only under the condition $n = kc/\omega \approx 1$ (see, e.g. Rafat *et al.* 2019*a*,*b*). As will be shown below, these conditions are not realized in the region of radiation generation. Therefore, the approximation $B \to \infty$ used in this paper, when for cold flow the dielectric permittivity tensor ε_{ij} reduces to

$$\varepsilon_{ij} = \begin{bmatrix} 1, & 0, & 0 \\ 0, & 1, & 0 \\ 0, & 0, & 1 - \dfrac{\omega_{\rm pe}^2}{\gamma^3 \tilde{\omega}^2} \end{bmatrix}, \tag{2.2}$$

is adequate to analyse the propagation effects for $\theta_b > \theta_{\rm rad}$.

Another consequence of this approximation is that we can restrict ourselves to a one-dimensional distribution function of particles $F(u)$ ($\int F(u)\,{\rm d}u = 1$), where $u = \beta\gamma$ is the particle four-velocity, $\beta = v_\parallel/c$, and $\gamma = (1-\beta^2)^{-1/2}$ ($v_\parallel$ is the velocity parallel to the magnetic field). As will be shown below, the waves under consideration either decay long before reaching the cyclotron resonance region, or pass through this region when their refractive indices do not differ from unity.

Further, the plasma number density can be determined as

$$N_e = \lambda N_{\rm GJ} \approx 0.7 \times 10^{12} \left(\frac{P}{1\ {\rm s}}\right)^{-1} \left(\frac{B_0}{10^{12}\ {\rm G}}\right) \left(\frac{\lambda}{10^4}\right) \left(\frac{l}{10R}\right)^{-3}\ {\rm cm}^{-3}. \tag{2.3}$$

Here

$$N_{\rm GJ} = \frac{\Omega B}{2\pi ce}, \tag{2.4}$$

is the Goldreich–Julian particle number density (the minimum value which is necessary to screen the longitudinal electric field),

$$\lambda = \frac{N_e}{N_{\rm GJ}} \sim 10^4, \tag{2.5}$$

is the pair production multiplicity (Daugherty & Harding 1982; Gurevich & Istomin 1985; Arendt & Eilek 2002; Medin & Lai 2010; Timokhin 2010; Timokhin & Harding 2015), $\Omega = 2\pi/P$ is the neutron star angular velocity, R is the stellar radius and l is the distance from the star centre. It should also be noted that we consider the areas located at distances l much smaller than the so-called light cylinder $R_L = c/\Omega$, where the magnetic field can be considered a dipole. Finally, the $\theta_{\rm cr}/\theta_{\rm rad}$ ratio discussed above ensuring the validity of our approximation $B \to \infty$, can be written in the form

$$\frac{\theta_{\rm cr}}{\theta_{\rm rad}} \approx 2 \times 10^{-4} \left(\frac{P}{1\ {\rm s}}\right)^{-1/2} \left(\frac{B_0}{10^{12}\ {\rm G}}\right)^{-1/2} \left(\frac{\lambda}{10^4}\right) \left(\frac{\gamma_s}{100}\right) \left(\frac{l}{10R}\right)^{3/2}. \tag{2.6}$$

As we can see, at distances $l \sim$ 10–100R, the approximation we use is valid.

As was shown by Beskin *et al.* (1988), dispersion properties of normal modes in the pulsar magnetosphere significantly depend on the parameter

$$A_p = \frac{\omega_{\rm pe}^2 \gamma_s}{\omega^2} \approx 0.56 \times 10^4 \left(\frac{P}{1\ {\rm s}}\right)^{-1} \left(\frac{B_0}{10^{12}\ {\rm G}}\right) \left(\frac{\lambda}{10^4}\right) \left(\frac{\gamma_s}{100}\right) \left(\frac{\nu}{1\ {\rm GHz}}\right)^{-2} \left(\frac{l}{10R}\right)^{-3}, \tag{2.7}$$

where $\omega_{\rm pe} = (4\pi e^2 N_e/m_e)^{1/2}$ is the plasma frequency and $\gamma_s \sim 100$ is the bulk Lorentz factor of the outflowing plasma. Here, we highlight that we do not use parameter A_p in exact formulae; we need it only for separating two asymptotic solutions. Therefore, our definition of this quantity is somewhat different from the definition given by Beskin *et al.* (1988): $A_p = \omega_{\rm pe}^2 \gamma_q/\omega^2$, where $\gamma_q = \langle 1/\gamma^3 \rangle^{-1/3}$ (for cold plasma, they naturally coincide).

For example, for $A_p \ll 1$ and for cold flow, the refractive index n_4 obtained from dispersion equation $\det(n^2\delta_{ij} - n_i n_j - \varepsilon_{ij}) = 0$ with dielectric tensor (2.2) for the ordinary O-mode ($j = 2$ in our notation for $A_p > 1$) in the limit $\theta_b \to 0$ looks like (see Beskin *et al.* 1988, (2.17)[1]; Rafat *et al.* 2019*b*, (6.17))

$$n_4 \approx 1 - 2\frac{\gamma_s \omega_{\rm pe}^2}{\omega^2}\theta_b^2. \tag{2.8}$$

On the other hand, for $A_p \gg 1$ we have $n_4 > 1$ (see below). Indeed, for low number density N_e (when $A_p \ll 1$), i.e. at large enough distances from a neutron star, plasma has little effect on the properties of the transverse waves, which makes us assume with great accuracy that the refractive indices for extraordinary (electric vector of the wave is perpendicular to the $(\boldsymbol{kB})$-plane, $j = 1$) and ordinary (electric vector of the wave belongs to the $(\boldsymbol{kB})$-plane, $j = 2$) modes $n_{1,2} \approx 1$. This implies that two orthogonal modes propagate rectilinearly in the pulsar magnetosphere.

On the other hand, the most non-trivial properties take place for $A_p \gg 1$, i.e. according to (2.7), just in the radio generation domain $r < 30$–$100R$. Indeed, according to Beskin *et al.* (1988), the expressions for the dependence of the refractive indices on the angle θ_b for all four normal waves look like

$$n_1 = 1, \tag{2.9}$$

$$n_2 \approx 1 + \frac{\theta_b^2}{4} - \left(\left\langle \frac{\omega_{\rm pe}^2}{\gamma^3\omega^2}\right\rangle + \frac{\theta_b^4}{16}\right)^{1/2}, \tag{2.10}$$

$$n_3 \approx 1 + \frac{\theta_b^2}{4} + \left(\left\langle \frac{\omega_{\rm pe}^2}{\gamma^3\omega^2}\right\rangle + \frac{\theta_b^4}{16}\right)^{1/2}, \tag{2.11}$$

$$n_4 \approx 1 + \frac{\theta_b^2}{2}. \tag{2.12}$$

Here the brackets $\langle \cdots \rangle$ denote the averaging on the distribution function $F(u)$, i.e. $\langle \cdots \rangle = \int \cdots F(u)\, {\rm d}u$. It should be noted that expression (2.12) for the wave $j = 4$ is approximate; the small additional term avoiding the singularity noted by Rafat *et al.* (2019*b*) will be found in § 5.

[1] In this formula, you need to take into account that $\tilde{\omega} = \omega - k v_\parallel \approx \omega/(2\gamma^2)$.

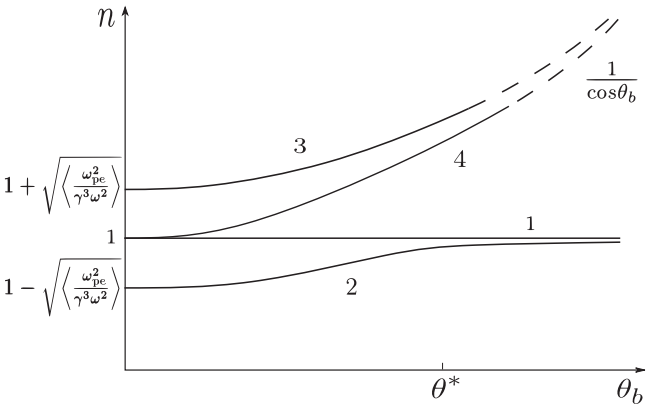

FIGURE 1. Normal modes for $A_p \gg 1$ and $a_p \ll 1$ with the refractive indices $n \approx 1$ propagating from the neutron star surface as a function of the angle θ_b between the wavevector $\boldsymbol{k}$ and the external magnetic field $\boldsymbol{B}$ (Beskin *et al.* 1988). Waves $j = 1$ (extraordinary X-mode) and $j = 2$ (ordinary O-mode) can escape the pulsar magnetosphere. Subluminal modes $j = 3, 4$ decay at large angles θ_b and cannot escape the pulsar magnetosphere.

As shown in figure 1, for $A_p \gg 1$ the mode $j = 2$ during its propagation transforms from a longitudinal wave for $\theta_b \to 0$ (where $n_2 < 1$) to a transverse ordinary mode with $n_2 \approx 1$ for larger angles. We emphasize once again that everywhere below, due to small distances from the neutron star $l \ll R_L$ in the analysis of dispersion relations, the angles θ_b , etc. will be assumed to be small.

Figure 1 shows that the mixing of longitudinal and transverse waves takes place at $\theta_b \sim \theta^*$, where

$$\theta^* = \left\langle \frac{\omega_{pe}^2}{\gamma^3\omega^2} \right\rangle^{1/4}. \tag{2.13}$$

If for small angles $\theta_b < \theta^*$, we deal with two transverse modes $n_1 \approx n_4 \approx 1$ and with two branches of plasma wave $n_{2,3} \approx 1 \pm a_p^{1/2}$, then at large angles $\theta_b > \theta^*$ we have two transverse modes with $n_1 \approx n_2 \approx 1$ and two Alfvén modes with $n_3 \approx n_4 \approx 1/\cos\theta_b$ propagating along magnetic field lines. As was already noted, these waves are to decay. It should be noted that for cold outflow where $\langle 1/\gamma^3 \rangle \approx \gamma_s^{-3}$ we have

$$A_p \approx (\theta^*\gamma_s)^4. \tag{2.14}$$

This evaluation is very useful. In particular, rewriting condition $\theta^*\gamma_s \gg 1$ in the form $\theta^* \gg \gamma_s^{-1}$, we come to another important conclusion that in the domain where $A_p \gg 1$ radiation is generated at the angles $\theta_b \ll \theta^*$.

As we see, another key parameter of our problem is

$$a_p = \left\langle \frac{\omega_{pe}^2}{\gamma^3\omega^2} \right\rangle$$
$$\approx 0.56 \times 10^{-4} \left(\frac{P}{1\ \mathrm{s}}\right)^{-1} \left(\frac{B_0}{10^{12}\ \mathrm{G}}\right) \left(\frac{\lambda}{10^4}\right) \left(\frac{\gamma_s}{100}\right)^{-3} \left(\frac{\nu}{1\ \mathrm{GHz}}\right)^{-2} \left(\frac{l}{10R}\right)^{-3}. \tag{2.15}$$

In particular, the mode $j = 2$ cannot propagate outward for $a_p > 1$, i.e. for small enough frequencies ω. But for $a_p \ll 1$ (and, as was already stressed, only for $A_p \gg 1$ in the

radiation point), it is this wave that escapes the pulsar magnetosphere and is observed as an ordinary O-mode (see figure 1). For this reason, we consider its properties in detail in § 3.

Once again, we emphasize that the above expressions (2.9)–(2.12) for the refractive indices, $n_{1,2,3,4}$ were obtained under definite restrictions. In addition to condition $A_p \gg 1$, it was also assumed that the thermal spread over longitudinal momentum $p = m_e c u$ is sufficiently small, so that the averaging over the distribution function $F(u)$ does not cover resonant condition $\omega - k_\parallel v_\parallel = 0$, i.e.

$$1 - n\beta \cos\theta_b = 0. \tag{2.16}$$

This last circumstance was, in fact, a stumbling block. Indeed, the exact dispersion equation for an infinite magnetic field, but now for arbitrary energy distribution $F(u)$, looks like (Beskin *et al.* 1988; Rafat *et al.* 2019*b*)

$$(1 - n^2)\left(1 - n^2 + (1 - n^2\cos^2\theta_b)\frac{\omega_{\rm pe}^2}{\omega^2 n\cos\theta_b}\int \frac{1}{(1 - n\beta\cos\theta_b)}\frac{{\rm d}F}{{\rm d}u}\,{\rm d}u\right) = 0. \tag{2.17}$$

On the other hand, expressions (2.9)–(2.12) for the refractive indices correspond to the cold plasma approximation, when we can take velocity v out of the integration sign. But in reality, the distribution function of secondary particles $F(u)$ is wide enough (Daugherty & Harding 1982; Gurevich & Istomin 1985; Arendt & Eilek 2002; Medin & Lai 2010; Timokhin 2010; Timokhin & Harding 2015). Therefore, correction for the superluminal mode $j = 2$ and, all the more, a possibility of the damping for subluminal modes $j = 3, 4$ requires a separate detailed consideration (Rafat *et al.* 2019*a*,*b*). However, we recall that the damping of subluminal modes itself, which at large angles propagate along the magnetic field and, therefore, cannot leave a neutron star magnetosphere, has never been questioned (Beskin *et al.* 1988).

Obviously, for a quantitative study of thermal effects we must specify the distribution function $F(u)$. As was shown by Arendt & Eilek (2002), the distribution of secondary particles in the plasma rest frame with good accuracy can be approximated by the Jüttner distribution

$$F'(u') = \frac{\exp(-\rho\gamma')}{2K_1(\rho)}, \tag{2.18}$$

with parameter $\rho = m_e c^2/T \approx 1$. Here K_1 is the Macdonald function of order one. This implies relativistic temperature $T \approx m_e c^2$. Accordingly, in the laboratory (neutron star) reference frame we have

$$F(u) = \frac{\exp[-\rho\gamma_s\gamma(1 - \beta\beta_s)]}{2K_1(\rho)}\gamma_s(1 - \beta\beta_s). \tag{2.19}$$

Note that, in contrast to Rafat *et al.* (2019*b*), we consider normalization $\int F(u)\,{\rm d}u = 1$. However, below we consider a wider class of distribution functions $F(u)$, since the distribution function (2.19) does not always adequately describe the distribution of secondary particles outflowing from the magnetosphere of a neutron star.

Thus, the goal of our study is to clarify how the thermal effects affect the propagation properties of radio waves in the pulsar magnetosphere. Therefore, in contrast to the works of Rafat *et al.* (2019*a*) and Rafat *et al.* (2019*b*), our main task is to analyse the dependence of their refractive indices n on the angle θ_b. It is clear that in the infinite magnetic field approximation (2.17) considered here, the extraordinary X-mode $j = 1$ remains unchanged.

Indeed, as the electric vector of this wave is perpendicular to the external magnetic field, this mode cannot interact with plasma particles. As a result, we have $n_1 = 1$, i.e. this mode propagates rectilinearly in the pulsar magnetosphere. For this reason, we discuss only three other modes.

3. Superluminal O-mode

At first, let us consider the O-mode $j = 2$; remember that here we consider the case $A_p \gg 1$. As shown in figure 1, for this wave $n_2 < 1$, i.e. it is a superluminal mode. Using the standard Lorentz transformation to the plasma rest frame

$$n' \cos\theta'_b = \frac{n\cos\theta_b - \beta_s}{1 - n\beta_s \cos\theta_b}, \tag{3.1}$$

we obtain for $\gamma_s \gg 1$, $A_p \gg 1$, and $\theta_b = 0$,

$$n'_2 \approx -1 + \frac{1}{(1-n_2)\gamma_s^2} \approx -1 + A_p^{-1/2}. \tag{3.2}$$

As $\omega' = \gamma_s\omega(1 - n_2\beta) > 0$, one can conclude that for $\theta_b = 0$ in the plasma rest frame the O-mode $j = 2$ corresponds to superluminal branch of a plasma wave propagating to the star surface.

On the other hand, as for the superluminal O-mode, the denominator in (2.17) is positive for all particle four-velocities u, one can obtain using integrating by parts,

$$1 - n_2^2 - (1 - n_2^2\cos^2\theta_b)\frac{\omega_{\rm pe}^2}{\omega^2}\left\langle \frac{1}{\gamma^3(1 - n_2\beta\cos\theta_b)^2}\right\rangle = 0. \tag{3.3}$$

For cold plasma (and for $|n - 1| \gg |\beta - 1|$, which is just true for $A_p \gg 1$) one can put $\beta = 1$, and we return to (2.10). On the other hand, for a wide enough distribution function, i.e. for parameter $\rho \sim 1$ incoming into the Jüttner distribution function (2.18), the value of β under the integral sign cannot be considered constant, and therefore a more detailed study is required.

Figure 2 shows how the refractive index n_2 depends on the angle θ_b for $A_p \gg 1$ for different parameters ρ (solid lines). The dashed lines correspond to the simplified expression (2.10) used by Beskin *et al.* (1988), where during the integration on du in (2.17) the condition $\beta = 1$ was assumed.

As we see, for $\rho \sim 1$ the difference in the refractive index from unity is already three to four times larger than that for cold plasma. It should be also emphasized that even for hot enough plasma (i.e. for $\rho \sim 1$) the simplified evaluation (2.10) reproduces a good enough dependence of the refractive index n_2 on angle θ_b. Note that in this figure, the angle θ_b is expressed in terms of θ^*, which is different for different frequencies ω.

Remember that it is the wave $j = 2$ that escapes from the pulsar magnetosphere as the ordinary O-mode (Barnard & Arons 1986; Beskin & Philippov 2012). In this case, the difference in the refractive index from unity leads to a deviation of the wave from the magnetic axis. As a result, the mean profile formed by the O-mode turns out to be wider than for the extraordinary X-mode $j = 1$.

To obtain the width of the directivity pattern W_r, we must now determine the propagation path of the O-mode. As was shown by Beskin *et al.* (1988), for small angles $\theta_\perp = k_\perp/k \ll 1$ and $\alpha = (3/2)r_\perp/l \ll 1$ where α is the angle between the magnetic field and the magnetic axis, and $r_\perp$ and $k_\perp$ are the components of the vectors perpendicular

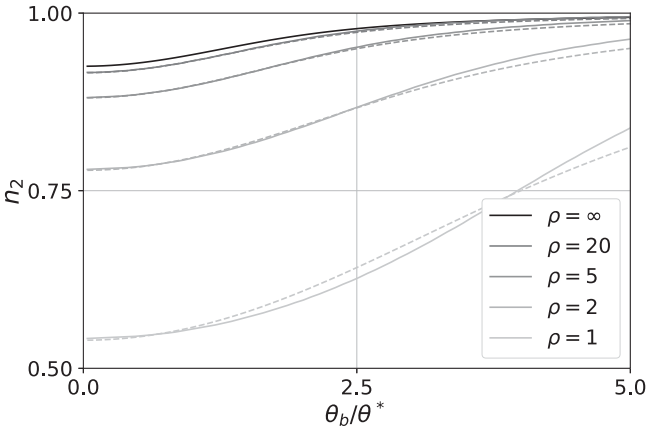

FIGURE 2. Dependence of refractive index n_2 on the angle θ_b for different parameters $\rho = m_e c^2/T$ for $\gamma_s = 100$, $\lambda = 10^4$, $P = 1$ s, $B = 10^{11}$ G and $\nu = 1$ GHz ($A_p \sim 10^6$). The solid lines correspond to numerical solution of (3.3) and the dashed lines correspond to analytical expression (2.10) for different parameters ρ.

to the magnetic axis, in dipole magnetic field the equations of geometric optics $\mathrm{d}\boldsymbol{r}/\mathrm{d}t = \partial\omega/\partial\boldsymbol{k}$, $\mathrm{d}\boldsymbol{k}/\mathrm{d}t = -\partial\omega/\partial\boldsymbol{r}$ are reduced to the following system:

$$\frac{\mathrm{d}r_\perp}{\mathrm{d}l} = \frac{\theta_\perp}{n} - \frac{1}{n^2}\frac{\partial n}{\partial\theta_b}, \tag{3.4}$$

$$\frac{\mathrm{d}\theta_\perp}{\mathrm{d}l} = \frac{3}{2}\frac{1}{n^2 l}\frac{\partial n}{\partial\theta_b}. \tag{3.5}$$

Here l is the distance from the star centre, and we use relations $\theta_b = \alpha - \theta_\perp$ and $\mathrm{d}l/\mathrm{d}t = c$.

Differentiating now the second bracket in the dispersion equation (2.17) with respect to θ_b, we obtain for the derivative $\partial n_2/\partial\theta_b$,

$$\frac{\partial n_2}{\partial\theta_b} = \theta_b\frac{A}{1+A}, \tag{3.6}$$

where

$$A = 4\frac{\omega_{\mathrm{pe}}^2}{\omega^2}\left\langle\frac{u(2u^2\xi - 1)}{(2u^2\xi + 1)^3}\right\rangle \tag{3.7}$$

and $\xi = 1 - n_2 - \theta_b^2/2$ is to be the root of the dispersion equation

$$\xi - \frac{\theta_b^2}{2} = 4\frac{\omega_{\mathrm{pe}}^2}{\omega^2}\left\langle\frac{u\xi}{(2u^2\xi + 1)^2}\right\rangle. \tag{3.8}$$

As was already mentioned, we present all the expressions in the limit of $\theta_b \ll 1$ and $|n - 1| \ll 1$.

In the limit $u^2\xi \gg 1$ we reduce to 'hydrodynamical' relations

$$\frac{\mathrm{d}r_\perp}{\mathrm{d}l} = \theta_\perp + \frac{(\alpha - \theta_\perp)}{2}\left[1 - \frac{(\alpha - \theta_\perp)^2}{[16a_p(l) + (\alpha - \theta_\perp)^4]^{1/2}}\right], \tag{3.9}$$

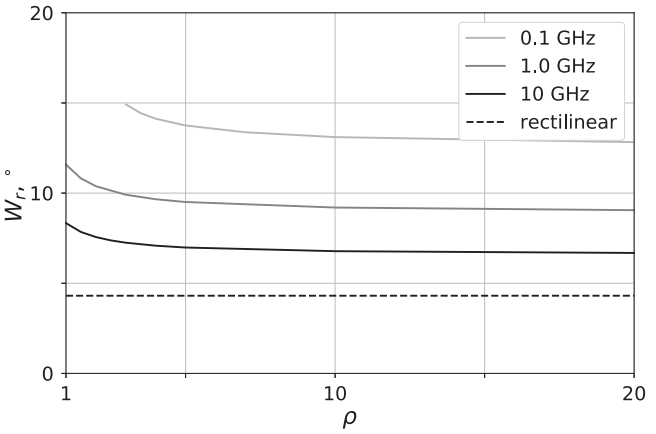

FIGURE 3. Dependence of the width of the directivity pattern W_r (3.11) (in degrees) on parameter $\rho = m_e c^2/T$ for $\gamma_s = 100$, $\lambda = 10^4$, $P = 1$ s, magnetic field on the star surface $B_0 = 10^{12}$ G and for starting point $l = 3R$. The dashed line corresponds to rectilinear propagation.

$$\frac{\mathrm{d}\theta_\perp}{\mathrm{d}l} = \frac{3}{4}\frac{(\alpha - \theta_\perp)}{l}\left[1 - \frac{(\alpha - \theta_\perp)^2}{[16a_p(l) + (\alpha - \theta_\perp)^4]^{1/2}}\right], \tag{3.10}$$

obtained by Beskin *et al.* (1988). Here a_p is given by relation (2.15) and n_2 is to be found as a solution of (3.3). Note that during integration it is necessary to take into account the dependence of $a_p = \langle\omega_{\mathrm{pe}}^2/(\gamma^3\omega^2)\rangle$ via ω_{pe} on l (figure 2 shows the dependence of the refractive index n_2 on the angle θ_b at a given point, not along the beam propagation). As a result, integrating the system of (3.4) and (3.5), we obtain for the width of the directivity pattern

$$W_r = 2\theta_\perp(\infty). \tag{3.11}$$

The dependence of the width of the directivity pattern W_r (3.11) on parameter ρ is shown in figure 3 for the same parameters as in figure 2; we start at the point $l = 3R$, where $\theta_\perp = \alpha$ (radiation along the magnetic field line). The dashed line corresponds to rectilinear propagation when $W_r = 2\,\alpha(3R)$. As we see, thermal effects do not significantly affect the width of the directivity pattern.

A detailed study of the effects of the refraction of an ordinary wave on the formation of mean profiles of radio pulsars will be carried out in a separate work. At the same time, it should be emphasized that the starting radius $l = 3R$ used in this work was selected taking into account the observational data. Indeed, according to the statistical analysis performed by Rankin (1990) and Maciesiak, Gil & Melikidze (2012), the intrinsic pulse width W_r for the core component (just corresponding to X-mode in our classification) is equal to $W_r = W_0/P^{1/2}$, where $W_0 = 2^\circ$–3°. Assuming that this value corresponds to the opening magnetic field lines $3(\Omega l/c)^{1/2}$ at the distance l, we obtain for the height of the radio emission $l \sim 3$ stellar radius. As for the cases when the observed pulse width turns out to be larger than these values (see, for example, Mitra 2017), this, as is well known, can be associated either with non-orthogonality (when the observable pulse width $W_{\mathrm{obs}} = W_r/\sin\chi$) or with the fact that the average profile is determined by the O-mode $j = 2$. We can note that under the condition $\rho \gg 1$, the dependence of the window width

W_r on the frequency ν shown in figure 2 with good accuracy satisfies the dependence

$$W_r \approx 8^\circ \left(\frac{\nu}{1\ \mathrm{GHz}}\right)^{-0.14} \left(\frac{P}{1\ \mathrm{s}}\right)^{-0.43} \left(\frac{B_0}{10^{12}\ \mathrm{G}}\right)^{0.07} \left(\frac{\gamma_s}{100}\right)^{-0.11} \left(\frac{\lambda}{10^4}\right)^{0.07} \left(\frac{l}{3R}\right)^{0.15}, \tag{3.12}$$

predicted by Beskin *et al.* (1988) for an O-mode for $P = 1$ s, $\lambda = 10^4$ and $l = 3R$. For more realistic temperatures $\rho \sim 1$, the pulse width is to be even larger.

In conclusion, we note that, according to relation (2.7), for frequencies $\nu = \omega/2\pi \sim 1$ GHz in the region of radio emission generation $l < 100R$ ($A_p > 1$), the refractive index n_2 (2.10) differs significantly from unity. On the other hand, as was shown by Rafat *et al.* (2019*a*), mode crossing occurs only if the refractive index n is close to unity (in the plasma rest frame $|n^2 - 1| \sim \omega_{\mathrm{pe}}^2/\omega_B^2$). Hence, such an intersection of modes is possible only in an insignificant range of heights $l \sim 100R$ ($A_p \sim 1$), when in the hydrodynamic limit one should use the more accurate expression

$$n_2 \approx 1 + \frac{1}{2\gamma_s^2} - \left(\frac{\omega_{\mathrm{pe}}^2}{\gamma_s^3 \omega^2}\right)^{1/2}, \tag{3.13}$$

giving the possibility of fulfilling the condition $n_2 \approx 1$. On the other hand, at the distances $l \sim 10R$ such crossing takes place for frequencies $\nu > 100$ GHz only.

Thus, for frequencies $\nu \sim 1$ GHz the mode crossing cannot take place for the O-mode in the generation region. As far as the heights $l \sim 100R$, the O-mode passes this region at much higher angles $\theta_b \gg \theta_{\mathrm{cr}}$. Therefore, for the O-mode $j = 2$ emitted in the region $l \ll 100R$ the influence of thermal effects in the region of mode crossing can be neglected.

4. Subluminal plasma-Alfvén mode

Now, let us consider mixing plasma-Alfvén mode $j = 3$ ($n_3 > 1$, see figure 1); again, we consider the case $A_p \gg 1$. For this mode for $\theta_b = 0$ we have

$$n_3' \approx -1 + \frac{1}{(1 - n_3)\gamma_s^2} \approx -1 - A_p^{-1/2} \tag{4.1}$$

and $\omega' = \gamma_s \omega (1 - n_2 \beta) < 0$. Thus, for $\theta_b = 0$ in the plasma rest frame this mode corresponds to the subluminal branch of a plasma wave also propagating to the star's surface. On the other hand, for large enough angles θ_b in the laboratory frame, (2.11) gives $n_3 \approx 1 + \theta_b^2/2 \approx 1/\cos\theta_b$. This dispersion equation corresponds to an Alfvén mode propagating along the magnetic field line.

It is clear that the main difference between the subluminal ($j = 3$) and the superluminal ($j = 2$) wave is that it becomes possible to perform the Cherenkov resonance condition (2.16). In this case, since we consider the problem of wave propagation in a curved external magnetic field when the angle θ_b changes along the propagation path, the resonance condition is to be fulfilled even for cold plasma. That is why in figure 1 it is the angle θ_b that is chosen as the main parameter.

However, for cold plasma, the resonance condition (2.16) occurs for the angles θ_b larger than the angle θ^*. This result can be obtained immediately if we write down the resonance condition in the form $(n - 1) - 1/2\gamma^2 - \theta_b^2/2 = 0$. For $n_3 > 1 + (\omega_{\mathrm{pe}}^2/\gamma^3\omega^2)^{1/2}$ and for $A_p \gg 1$ we just obtain $\theta_{\mathrm{res}} > \theta^*$. Therefore, we can conclude that for cold plasma, the damping of the plasma-Alfvén mode occurs only for large enough angles θ_b (as shown in figure 1).

On the other hand, for a fairly wide distribution function $F(u)$, i.e. for $\rho > 1$, there are particles which are in resonance with the wave even for $\theta_b = 0$. For ultrarelativistic plasma ($\gamma_s \gg 1$) and for small angles $\theta_b \ll \theta^*$, the resonance condition can be written in the form $\gamma_{\rm res} \approx 1/\theta^*$. As a result, using relation (2.14), we obtain for the exponent $a(\gamma_{\rm res}) = \rho\gamma_s\gamma_{\rm res}(1 - \beta_s\beta_{\rm res})$ in the Jüttner distribution $F(u) \propto \exp(-a)$ for resonance particles:

$$a(\gamma_{\rm res}) \approx \rho\gamma_s\theta^* \sim \rho A_p^{1/4}. \tag{4.2}$$

Thus, for $A_p \gg 1$ the damping of the plasma-Alfvén mode for $\theta_b = 0$ is to be weak even for $\rho \sim 1$.

To determine the attenuation of the wave $j = 3$ for an arbitrary temperature, it is convenient to find the solution of the dispersion equation (2.17) in the form

$$n_3 \cos\theta_b = 1 + x_3. \tag{4.3}$$

Then for small angles $\theta_b \ll 1$, relativistic energies ($\beta \approx 1 - 1/(2u^2)$) and for $x_3 \ll 1$, we obtain

$$x_3\left(x_3 + \frac{\theta_b^2}{2}\right) = I_3(x_3), \tag{4.4}$$

where

$$I_3(x_3) = \frac{\omega_{\rm pe}^2}{\omega^2(1+x_3)}\left[\fint \frac{2u^2x_3^2}{(2u^2x_3 - 1)}\frac{{\rm d}F}{{\rm d}u}\,{\rm d}u + {\rm i}\pi\frac{x_3^{1/2}}{2\sqrt{2}}\frac{{\rm d}F}{{\rm d}u}\bigg|_{u=(2x_3)^{-1/2}}\right]. \tag{4.5}$$

Here, as usual, for small imaginary part ${\rm Im}\,n$ in comparison with its real part, the real part of the integral $\fint$ is to be taken in the sense of the principal value.

Besides, for small angles $\theta_b \ll \theta^*$, when according to (2.11) $n_3 \approx 1 + a_p^{1/2}$, our definition (4.3) gives $x_3 \approx a_p^{1/2}$. This evaluation can be easily obtained from condition $x_3 \approx I_3^{1/2}$ resulting from (4.4), if we neglect the second term in (4.5) and use the limit $x_3u^2 \gg 1$. The last relation results from evaluation $x_3u^2 \sim a_p^{1/2}\gamma_s^2 \sim A_p^{1/2}$. In particular, this implies that the resonant particles correspond to the low-energy part of the distribution function ($\gamma_{\rm res} \ll \gamma_s$). As a result, expanding the denominator in (4.5) by a small parameter $1/(2u^2x_3)$, we obtain that $I_3 = J_3$, where

$$J_3(x_3) = \frac{\omega_{\rm pe}^2}{\omega^2(1+x_3)}\fint x_3\left(1 + \frac{1}{2u^2x_3}\right)\frac{{\rm d}F}{{\rm d}u}\,{\rm d}u \approx \left\langle\frac{\omega_{\rm pe}^2}{\gamma^3\omega^2}\right\rangle, \tag{4.6}$$

as the first integration term vanishes due to the identity $\int({\rm d}F/{\rm d}u)\,{\rm d}u = 0$.

Here it is interesting to check the accuracy of the approximation under consideration. For this, in figure 4 we show a comparison of the ratios of the values x_3 obtained from relations (4.4) and (4.6) and from exact dispersion equation (2.17) for $\theta_b = 0$, $\lambda = 10^4$ and $\nu = 1$ GHz. As we see, a good enough agreement does exist for different starting points l.

We also note that there are no contradictions with the results presented by Rafat *et al.* (2019*b*), since the range of parameters we are considering (precisely due to condition $A_p > 1$) corresponds to the values $0 < \log_{10}\gamma_\phi' < 2$ (for $\gamma_s = 100$) where, according to their figure 11, the results actually match each other. Wherein, the accuracy of the approximation becomes worse as $A_p \to 1$ ($\gamma_\phi' \to \gamma_s$).

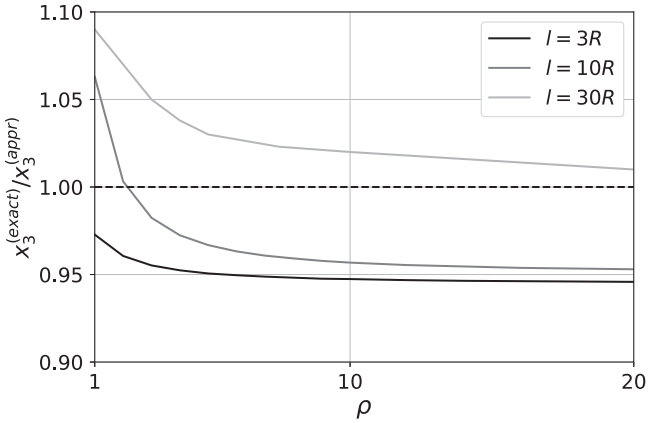

FIGURE 4. Comparison of the ratio of values $x_3^{(\mathrm{exact})}/x_3^{(\mathrm{appr})}$ obtained from relations (4.4) and (4.6) and from exact dispersion equation (2.17) for different starting points.

Further, one can see that the leading (real) term in I_3 actually does not depend on x. Therefore, for weak damping, the imaginary part of $n_3 \approx 1 + x_3 + \theta_b^2/2$ is completely determined by the second term,

$$\mathrm{Im}\, n_3 = \frac{\pi}{2\sqrt{2}} \frac{\omega_{\mathrm{pe}}^2}{\omega^2} \frac{[(16J_3 + \theta_b^4)^{1/2} - \theta_b^2]^{1/2}}{(16J_3 + \theta_b^4)^{1/2}} \frac{\mathrm{d}F}{\mathrm{d}u}\bigg|_{u=(2x_3)^{-1/2}}, \tag{4.7}$$

since the resonance condition is achieved in the low-energy region, where $\mathrm{d}F/\mathrm{d}u > 0$. Nevertheless, $\mathrm{Im}\, n_3 > 0$, which corresponds to the attenuation of the wave $j = 3$. This is due to the fact that the wave frequency is negative in the plasma rest reference frame (see appendix A for more detail).

Figure 5 shows the levels $l = r_d$ at which the optical depth, for the mode $j = 3$,

$$\tau = \frac{\omega}{c} \int_{l=r_0}^{l=r_d} \mathrm{Im}\, n_3 \, \mathrm{d}l, \tag{4.8}$$

becomes equal to unity. Integration was carried out using general relations (3.4)–(3.5) resulting in (Beskin *et al.* 1988)

$$\frac{\mathrm{d}r_\perp}{\mathrm{d}l} = \theta_\perp + \frac{(\alpha - \theta_\perp)}{2}\left[1 + \frac{(\alpha - \theta_\perp)^2}{[16a_p(l) + (\alpha - \theta_\perp)^4]^{1/2}}\right], \tag{4.9}$$

$$\frac{\mathrm{d}\theta_\perp}{\mathrm{d}l} = \frac{3}{4}\frac{(\alpha - \theta_\perp)}{l}\left[1 + \frac{(\alpha - \theta_\perp)^2}{[16a_p(l) + (\alpha - \theta_\perp)^4]^{1/2}}\right]. \tag{4.10}$$

As in all the previous figures, we set the radiation radius to $r_0 = 3R$. The solid lines correspond to the ratio $\theta_b/\theta^* < 1$ at the level $\tau = 1$, and the dashed-dotted lines correspond to the ratio $\theta_b/\theta^* > 1$.

As we can see, even for $\rho = 1$ the wave damps at the heights significantly higher than the radiation level. Therefore, there is no doubt in the very existence of this wave. On the other hand, for $\rho \sim 1$ the damping occurs at the angles θ_b even smaller than local $\theta^*(l)$, so that the inclusion of thermal effects into consideration leads to the fact that this wave attenuates at much smaller distances from a neutron star in comparison with the case of cold plasma.

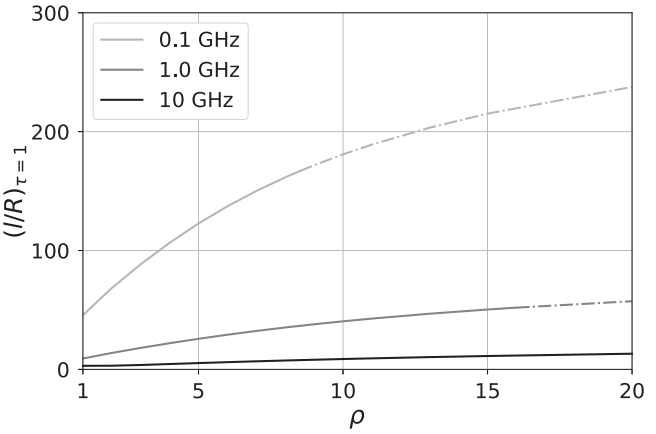

FIGURE 5. Levels $l = r_d$ at which the optical depth τ (4.8) for mode $j = 3$ becomes equal to one for the same parameters as in figure 3. The solid lines correspond to the ratio $\theta_b/\theta^* < 1$ at the level $\tau = 1$ and the dashed-dotted lines correspond to the ratio $\theta_b/\theta^* > 1$.

5. Subluminal Alfvén mode

Finally, let us consider the Alfvén mode $j = 4$. For $\theta_b = 0$ it corresponds to the transverse ordinary O-mode ($n_4 = 1$), but for large enough θ_b (and again for $A_p \gg 1$) we obtain $n_4 \approx 1/\cos\theta_b$, i.e. this mode also propagates along the magnetic field line. Unlike the mode $j = 3$, for the mode $j = 4$ the resonance condition cannot be satisfied for $\theta_b = 0$. However, it becomes possible for $\theta_b > 0$, the resonant particles having the energies much larger than the average energy of outflowing plasma ($\gamma_{\rm res} \gg \gamma_s$).

Due to (2.12), for this mode it is also convenient to find the solution of the dispersion equation (2.17) in the form

$$n_4 \cos\theta_b = 1 + x_4. \tag{5.1}$$

Then for small angles $\theta_b \ll 1$ and relativistic energies ($\beta \approx 1 - 1/(2u^2)$), we obtain

$$x_4 = \frac{\theta_b^2/2}{I_4(x_4) - 1}, \tag{5.2}$$

where

$$I_4(x_4) = -\frac{\omega_{\rm pe}^2}{\omega^2}\left[\int \frac{2u^2}{1 - 2u^2 x_4}\frac{{\rm d}F}{{\rm d}u}\,{\rm d}u - {\rm i}\pi\frac{x_4^{-3/2}}{2\sqrt{2}}\frac{{\rm d}F}{{\rm d}u}\bigg|_{u=(2x_4)^{-1/2}}\right]. \tag{5.3}$$

Here, in contrast to (4.5), for the Alfvén mode $j = 4$ we have $x_4 u^2 \ll 1$. Indeed, neglecting $2u^2 x_4$ in the denominator and the second term in (5.3), we obtain for small angles θ_b

$$x_4 = \frac{\theta_b^2/2}{J_4 - 1}, \tag{5.4}$$

where

$$J_4 = 4\frac{\omega_{\rm pe}^2\langle u\rangle}{\omega^2} \approx 4A_p. \tag{5.5}$$

As a result, we obtain $x_4 u^2 \sim \gamma_s^2\theta_b^2/A_p$, so that up to the angles $\theta_b \sim \theta^*$ we have $x_4 u^2 < A_p^{-1/2}$ due to (2.14).

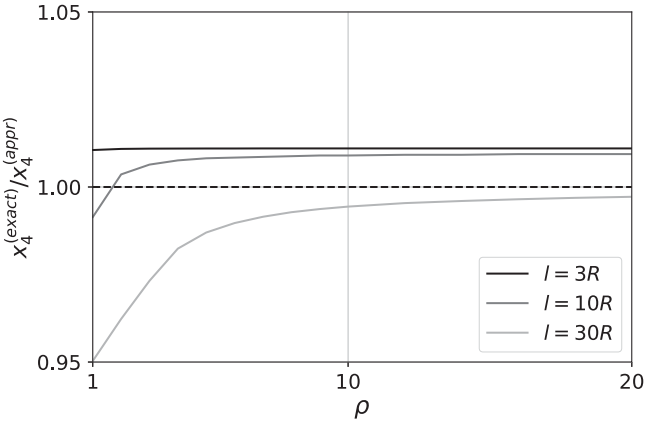

FIGURE 6. Comparison of the ratio of values $x_4^{(\mathrm{exact})}/x_4^{(\mathrm{appr})}$ obtained from relations (5.4)–(5.5) and from exact dispersion equation (2.17) for different starting points.

Figure 6 shows a comparison of the ratios of the values x_4 obtained from relations (5.4) and from exact dispersion equation (2.17) for $\theta_b = 0.02$, $\lambda = 10^4$ and $\nu = 1$ GHz. As we see, a good agreement exists for different starting points l for Alfvén wave $j = 4$ as well. In particular, such a good agreement also shows that the corresponding root of the dispersion equation is far enough from the value $n = 1/\cos\theta_b$. Thus, the contradiction with the paper by Rafat *et al.* (2019*b*) is removed, where it was pointed out that the approach under consideration is not applicable for $n \approx 1/\cos\theta_b$.

Further, as $I_4(0) \approx 4A_p$, we can conclude that for $A_p \gg 1$ the disturbance x_4 to expression n_4 (2.12) is indeed small, with resonant particles being absent for $\theta_b = 0$. Certainly, as previously mentioned, this expression can only be used if the second term in brackets in (5.3) is much smaller than the first term. As was already highlighted, this implies that for this mode the resonant particles correspond to the high-energy part of the distribution function.

Finally, we see that the leading (real) term in J_4 again does not depend on our variable x_4. Therefore, for weak damping, the imaginary part of $n_4 \approx 1 + x_4 + \theta_b^2/2$ is completely determined by the second term

$$\mathrm{Im}\, n_4 = -\frac{\pi}{8}\,\frac{J_4^{1/2}}{\langle u\rangle\theta_b}\,\frac{\mathrm{d}F}{\mathrm{d}u}\bigg|_{u=(2x_4)^{-1/2}}. \tag{5.6}$$

Here we neglect the terms of the order of $A_p^{-1/2}$. Since now the resonance condition is achieved in the high-energy region, where $\mathrm{d}F/\mathrm{d}u < 0$, we again have $\mathrm{Im}\, n_4 > 0$ corresponding to attenuation of the wave $j = 4$.

Note that, in reality, the relation (5.2) has no singularity. Indeed, expanding I_4 as

$$I_4(x_4) = -\frac{\omega_{\mathrm{pe}}^2}{\omega^2}\int 2u^2(1 + 2u^2x_4)\frac{\mathrm{d}F}{\mathrm{d}u}\,\mathrm{d}u \approx 4\frac{\omega_{\mathrm{pe}}^2\langle u\rangle}{\omega^2} + 16\frac{\omega_{\mathrm{pe}}^2\langle u^3\rangle}{\omega^2}x_4 + \cdots \tag{5.7}$$

and assuming that $\omega_{\mathrm{pe}}^2\langle u^3\rangle/\omega^2 \approx J_4\gamma_s^2$ we obtain

$$x_4 \approx \frac{-(J_4 - 1) \pm [(J_4 - 1)^2 + 8\,J_4\gamma_s^2\theta_b^2]^{1/2}}{8\,J_4\gamma_s^2}, \tag{5.8}$$

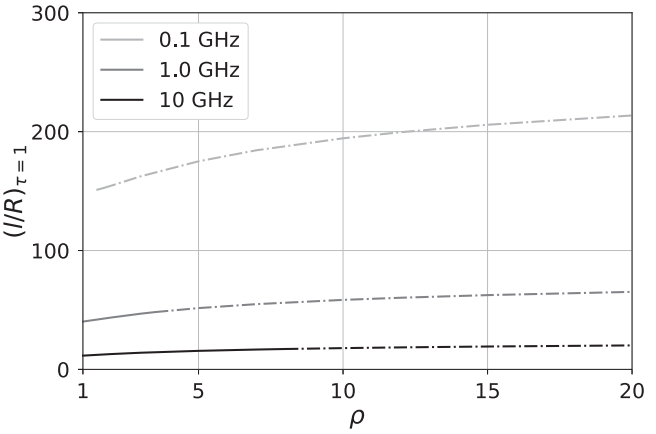

FIGURE 7. Same as in figure 5 for the Alfvén mode $j = 4$.

where the 'plus' sign corresponds to $J_4 > 1$, and the 'minus' sign to $J_4 < 1$. As a result, $n_4(\theta_b)$ always remains larger than unity if $J_4 > 1$ and *vice versa*. Thus, during the propagation the wave $j = 4$ never achieves the singularity $x_4 = 0$ (i.e. $n_4 \cos\theta_b = 0$), noted by Rafat *et al.* (2019*b*). On the other hand, for $A_p \ll 1$ ($I_4 \ll 1$) expression (5.2) results in

$$n_4 \approx 1 - 2\frac{\omega_{\rm pe}^2\langle u\rangle}{\omega^2}\theta_b^2, \tag{5.9}$$

which is in agreement with Beskin *et al.* (1988) and Rafat *et al.* (2019*b*).

Figure 7 shows the levels $l = r_d$ at which the optical depth τ becomes equal to unity for the mode $j = 4$. Integration was carried out using general relations (3.4)–(3.5) resulting in

$$\frac{{\rm d}r_\perp}{{\rm d}l} = \alpha, \tag{5.10}$$

$$\frac{{\rm d}\theta_\perp}{{\rm d}l} = \frac{3}{2}\frac{\theta_b}{l}. \tag{5.11}$$

As previously mentioned, we set the radiation radius to $r_0 = 3R$. The solid lines correspond to the ratio $\theta_b/\theta^* < 1$ at the level $\tau = 1$ and the dashed-dotted lines correspond to the ratio $\theta_b/\theta^* > 1$. As we see, thermal effects for the Alfvén wave $j = 4$, in general, are the same as for the wave $j = 3$. Again, even for $\rho = 1$ the wave damps at the heights significantly higher than the radiation level. On the other hand, for $\rho \sim 1$ the damping can occur at angles θ_b even smaller than local transition angle $\theta^*(l)$. The characteristic values for concentration N_e turn out to be four orders of magnitude lower than those for ordinary pulsars. As can be seen from relations (2.7) and (2.15), the values of A_p and a_p should be smaller in the same proportion.

6. Alternative distribution function

As was already stated, the Jüttner distribution function (2.19) may not accurately describe the real distribution function of particles flowing along open magnetic field lines in the pulsar magnetosphere. Here we rely on the results obtained under the analysis of processes of secondary electron–positron plasma generation in the polar magnetosphere of radio pulsars obtained by Gurevich & Istomin (1985). For this reason, we consider

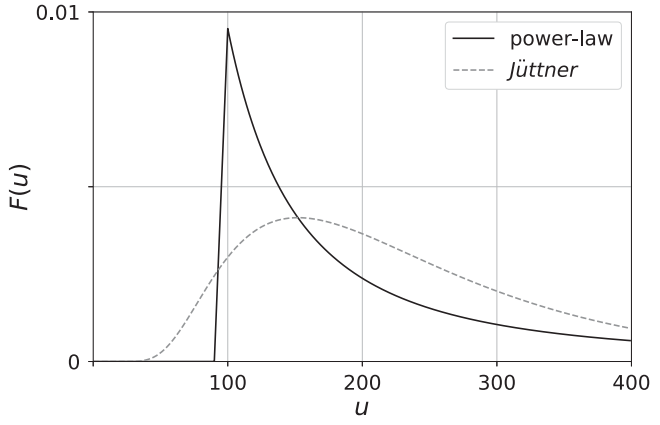

FIGURE 8. Particle distribution function $F(u)$ (6.1) in the laboratory frame, $u_0 = 100$, $\Delta = 10$. The dashed curve represents the Jüttner function with $\rho = 4$ in the frame moving with the Lorentz factor $\gamma_s = 210$.

another particle distribution function in the laboratory frame (see figures 8 and 9):

$$F(u) = \begin{cases} 0, & u < u_0 - \Delta, \\ \dfrac{u - u_0 + \Delta}{\Delta(u_0 + \Delta/2)}, & u_0 - \Delta < u < u_0, \\ \dfrac{u_0^2}{(u_0 + \Delta/2)} u^{-2}, & u > u_0. \end{cases} \tag{6.1}$$

Accordingly, the derivative of the distribution function over u is

$$\frac{\mathrm{d}F(u)}{\mathrm{d}u} = \begin{cases} 0, & u < u_0 - \Delta, \\ \dfrac{1}{\Delta(u_0 + \Delta/2)}, & u_0 - \Delta < u < u_0, \\ -\dfrac{2u_0^2}{(u_0 + \Delta/2)} u^{-3}, & u > u_0. \end{cases} \tag{6.2}$$

In addition, we will discuss in more detail the dispersion properties of the waves propagating in the pulsar magnetosphere, and we will not limit ourselves to small angles $\theta_b \ll 1$.

First, let us make some remarks regarding the choice of an alternative distribution function $F(u)$ (6.1). It is clear that the particle distribution function in the magnetosphere in the laboratory frame is a streaming function, i.e. there are no particles with negative momentum u. In addition, the cascade production of electrons and positrons from high to low energies ends even at rather high momenta, $u \simeq 10^2$. Therefore, the particle distribution function is zero for $u < u_0$.

However, in order to exclude the possible influence of the infinite derivative $\mathrm{d}F/\mathrm{d}u$ in the region $u \simeq u_0$, we made the transition from $F = 0$ to $F \propto u^{-2}$ for $u > u_0$ smooth, introducing the transition region $u_0 - \Delta < u < u_0$, where the derivative is finite. Bearing in mind that the distribution function is continuous at $u = u_0$ and the condition $\int F(u)\,\mathrm{d}u = 1$, we obtain the representation of $F(u)$ in the form (6.1).

It should be noted that this distribution function in the rest system, where $\langle v \rangle = \int F'(u')u'[1 + (u')^2]^{-1/2}\mathrm{d}u' = 0$, is not symmetric with respect to $u = 0$ (see figure 9).

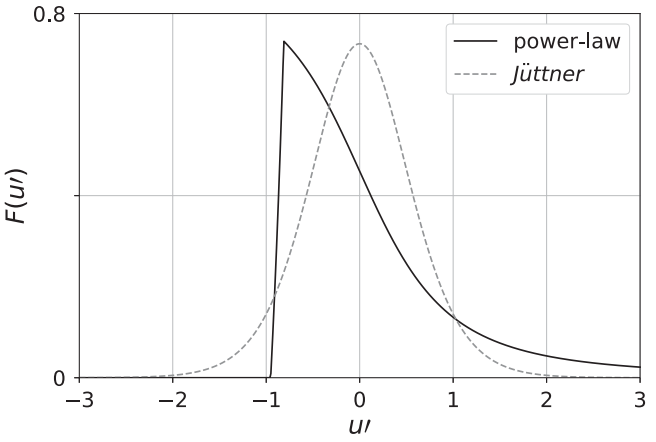

FIGURE 9. Particle distribution function $F(u')$ (6.1) in the rest frame, where the mean velocity is equal to zero. The Lorentz factor of motion of this frame is $\gamma_s = 210$. The dashed line shows the Jüttner function (2.18) with $\rho = 4$.

And although the maximum values of this function and the Jüttner function (2.18) with the parameter $\rho = 4$ match each other, and therefore the widths of the functions coincide, the general form of the functions is quite different. A particular difference is that the derivative $\mathrm{d}F'(u')/\mathrm{d}u'$ is negative for $u' < 0$. For the Jüttner distribution function this is not so. Negative values of the derivative $\mathrm{d}F'(u')/\mathrm{d}u'(u' < 0)$ could lead to instability in the rest system, although, as we will see below, the distribution function (6.1) is stable in the laboratory coordinate system and leads to damping of the 'Alfvén' waves. This suggests that we deal with convective stability/instability, which depends on the frame (Landau & Lifshits 1981).

Further, remember that the power-law dependence of the distribution function $F(u)$ (6.1) on the momentum u in the form $F(u) \propto u^{-2}$ for $u > u_0$ follows from numerical calculations of cascade generation of electron–positron plasma in the polar region of the pulsar magnetosphere first performed by Daugherty & Harding (1982) and subsequently confirmed by Gurevich & Istomin (1985). The characteristic value of u is $u_0 \simeq 10^2$, and $\Delta \ll u_0$. The value of Δ defines the region of arising of the distribution function from zero to its maximum value at $u = u_0$. Finally, it is necessary to stress that the Lorentz boost transformation to the plasma rest frame ($\langle v \rangle = 0$) corresponds to $\gamma_s \approx 2u_0$ (see figure 9).

Since in the laboratory reference frame $u \gg 1$, we can put $\beta = 1 - 1/(2u^2)$. As a result, dispersion equation (2.17) can be rewritten as

$$1 - n^2 + \frac{1 + n\cos\theta_b}{n\cos\theta_b}\frac{\omega_{\mathrm{pe}}^2}{\omega^2}\int\left[1 + \frac{n\cos\theta_b}{2u^2(1 - n\cos\theta_b)}\right]^{-1}\frac{\mathrm{d}F}{\mathrm{d}u}\,\mathrm{d}u = 0. \tag{6.3}$$

If

$$|n\cos\theta_b - 1| > \frac{n\cos\theta_b}{2(u_0 - \Delta)^2}, \tag{6.4}$$

(which is possible for $A_p \gg 1$), the denominator in the integrand does not turn to zero (there is no resonance), and we can go from integration over the derivative of the

distribution function to integration over the distribution function itself,

$$\int \left[1+\frac{n\cos\theta_b}{2u^2(1-n\cos\theta_b)}\right]^{-1}\frac{\mathrm{d}F}{\mathrm{d}u}\,\mathrm{d}u=-\left\langle\frac{n\cos\theta_b}{u^3(1-n\cos\theta_b)}\left[1+\frac{n\cos\theta_b}{2u^2(1-n\cos\theta_b)}\right]^{-2}\right\rangle. \tag{6.5}$$

Neglecting now the small term in brackets in the second equality of the (6.5), which is proportional to u^{-2}, we obtain for the dispersion equation

$$1-n^2-\frac{1+n\cos\theta_b}{1-n\cos\theta_b}a'_p=0, \tag{6.6}$$

where now $a'_p=\langle\omega_{\mathrm{pe}}^2/(u^3\omega^2)\rangle\approx a_p$. For the distribution function $F(u)$ (6.1), we obtain for $\Delta\ll u_0$

$$a'_p=\frac{1}{4}\frac{\omega_{\mathrm{pe}}^2}{u_0^3\omega^2}. \tag{6.7}$$

Thus, for $u\gg 1$ dispersion equation (6.3) is reduced to a cubic equation

$$n^3-\frac{1}{\cos\theta_b}n^2-(1+a'_p)n+\frac{1-a'_p}{\cos\theta_b}=0, \tag{6.8}$$

describing three electromagnetic modes propagating in the magnetosphere. Solving the cubic equation, we have

$$n_2=-\frac{(1-\sqrt{3}\,\mathrm{i})}{6}XZ^{-1/3}-\frac{(1+\sqrt{3}\,\mathrm{i})}{6}Z^{1/3}+\frac{1}{3\cos\theta_b}, \tag{6.9}$$

$$n_3=\frac{1}{3}(XZ^{-1/3}+Z^{1/3})+\frac{1}{3\cos\theta_b}, \tag{6.10}$$

$$n_5=-\frac{(1+\sqrt{3}\,\mathrm{i})}{6}XZ^{-1/3}-\frac{(1-\sqrt{3}\,\mathrm{i})}{6}Z^{1/3}+\frac{1}{3\cos\theta_b}, \tag{6.11}$$

where

$$X=3(1+a'_p)+\cos^{-2}\theta_b, \tag{6.12}$$

$$Y=\cos^{-3}\theta_b+9(2a'_p-1)\cos^{-1}\theta_b, \tag{6.13}$$

$$Z=(Y^2-X^3)^{1/2}+Y. \tag{6.14}$$

Two roots, n_2 and n_3, which were already obtained above, correspond to waves which propagate in the positive direction ($n>0$), and one extra mode $j=5$, which propagates in the negative direction ($n<0$).

For small values of the angle θ_b and the parameter a'_p ($\theta_b\ll 1, a'_p\ll 1$), dispersion equation (6.8) can be solved by substituting $n=1+\delta n$, where $\delta n\ll 1$. The solution is $\delta n=\theta_b^2/4\pm(\theta_b^4/16+a'_p)^{1/2}$, which just corresponds to the modes $j=2,3$ (2.10) and (2.11). However, we skip the third root of (6.8), which corresponds to the substitution $n=-1+\delta n$, where $\delta n=a'_p\theta_b^2/8$. This is the mode $j=5$. Previously, this mode was not taken into account, since only the waves propagating along the plasma flow were considered. It is clear that the waves propagating inwards, $n<0$, must have a refractive

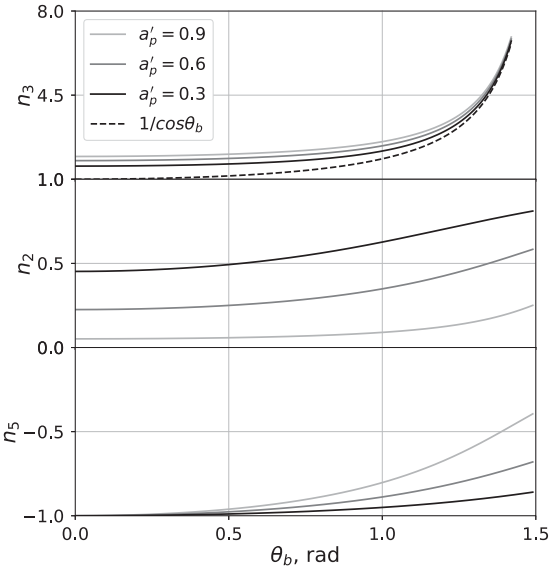

FIGURE 10. Refractive indices n for modes $j = 2, 3, 5$. The parameter $a'_p = \langle \omega_{\rm pe}^2/(u^3\omega^2)\rangle$. The dashed line corresponds to $n = 1/\cos\theta_b$.

index different from that of the waves propagating outwards. The wave $j = 5$ can be excited by a reverse current flowing in the polar region of the pulsar magnetosphere.

The dependencies of n_2, n_3 and n_5 on the angle θ_b are presented in figure 10. As was already shown, for $\theta_b = 0$ ($\cos\theta_b = 1$) we have $n_{2,3} = 1 \pm (a'_p)^{1/2}$. But for $\theta_b = \pi/2$, ($\cos\theta_b = 0$) we obtain $n_2 = (1 - a'_p)^{1/2}$ and $n_3 \to 1/\cos\theta$, the superluminal mode $j = 2$ transforming into a purely transverse wave. As for the wave $j = 5$, which was not mentioned earlier, it is a wave propagating in the negative direction in the laboratory reference frame, and is purely transverse: $n_5 = -1$ at $\theta_b = 0$ and $n_5 = -(1 - a'_p)^{1/2}$ at $\theta_b = \pi/2$. This mode occurs as a result of Lorentz transformation of the frequency and wavevector of a wave propagating in a positive direction in a rest frame into a laboratory frame.

Returning now to the question of wave attenuation, we note that for $\Delta \ll u_0$ the attenuation of the plasma-Alfvén wave $j = 3$, as for cold plasma, begins only at angles $\theta_b > \theta^*$. As for the attenuation of the Alfvén mode $j = 4$ ($n\cos\theta \simeq 1$), for this mode the second term in brackets in (6.3) cannot be neglected. As a result, the integral becomes equal to

$$\int \left[1 + \frac{n\cos\theta_b}{2u^2(1 - n\cos\theta_b)}\right]^{-1} \frac{{\rm d}F}{{\rm d}u}\,{\rm d}u = \int \frac{u^2}{u^2 - u_r^2 - {\rm i}0}\,\frac{{\rm d}F}{{\rm d}u}\,{\rm d}u. \tag{6.15}$$

Here the quantity u_r is the resonant momentum

$$u_r^2 = \frac{n\cos\theta_b}{2(n\cos\theta_b - 1)}, \tag{6.16}$$

and we added a small imaginary part in the denominator to take into account the Landau bypass rule for the pole ($\omega \to \omega + {\rm i}0$), i.e. for the refractive index $n \to n - {\rm i}0$. Thus, the

dispersion equation takes the form

$$1 - n^2 + \frac{\omega_{\rm pe}^2}{\omega^2}\frac{1 + n\cos\theta_b}{n\cos\theta_b}\left[\int \frac{u^2}{u^2 - u_r^2}\frac{{\rm d}F}{{\rm d}u}\,{\rm d}u + {\rm i}\frac{\pi u_r}{2}\frac{{\rm d}F}{{\rm d}u}\bigg|_{u=u_r}\right] = 0. \tag{6.17}$$

Substituting now the derivative ${\rm d}F/{\rm d}u$ from (6.2) and, again, introducing the notation

$$x = n\cos\theta_b - 1, \tag{6.18}$$

we obtain

$$\tan^2\theta_b + \frac{2x}{\cos^2\theta_b} - \frac{4\omega_{\rm pe}^2 u_0}{\omega^2}\left[\log\left(1 - \frac{1}{2xu_0^2}\right) - {\rm i}\pi\right]x = 0. \tag{6.19}$$

It should be borne in mind that the value x in the argument of the logarithm is a complex quantity. Therefore, the logarithm is complex also, and it does not contain a module in its argument.

As a result, one can see that for not very small angles $\theta_b > u_0^{-2} \simeq 10^{-4}$ and the condition $u_0^2\, a_p' \gg 1$ we obtain

$$x = {\rm i}\frac{\tan^2\theta_b}{4\pi}\frac{\omega^2}{u_0\omega_{\rm pe}^2}. \tag{6.20}$$

Thus, the imaginary part of the refractive index of the Alfvén mode is

$${\rm Im}(n_4\cos\theta_b) = \frac{\tan^2\theta_b}{4\pi}\frac{\omega^2}{u_0\omega_{\rm pe}^2} \simeq \frac{\tan^2\theta_b}{2\pi}A_p^{-1}, \tag{6.21}$$

which corresponds to the attenuation of the wave during its propagation in the magnetosphere.

Figure 11 shows how the levels $l = r_d$ at which the optical depth $\tau = 1$ (4.8) depend on parameter γ_s for both Jüttner ($\rho = 4$, γ_s) and power-law ($u_0 = \gamma_s/2$) distribution functions. As we see, these levels do not differ so drastically. This is due to the fact that in both cases the attenuation is determined by resonant particles whose energy is not much higher than the average particle energy.

Thus, in general, the properties of four normal waves depend weakly on the particle distribution function. On the other hand, we considered it necessary to stress here that in a magnetized, relativistic streaming plasma of the radio pulsar magnetosphere in the laboratory frame, i.e. in the frame associated with a neutron star, there are six modes depending on the polarization of the wave and the direction of their propagation. For $A_p \gg 1$ they are two transverse electromagnetic modes with the wave electric field polarization directed orthogonal to magnetic field with the refractive index ($n_1 = \pm 1$), two electromagnetic waves with polarization directed in the plane of the magnetic field and the wavevector (Alfvén wave with refractive index n_4, and the fifth mode with $n_5 < 0$) and two plasma waves with longitudinal polarization (along the magnetic field) at $\theta_b = 0$ and turning into transverse wave at $\theta_b = 90^\circ$ for n_2 and to Alfvén wave for n_3.

It should be also noted that for a symmetric distribution function $F(u)$ with respect to the zero momentum, $u = 0$, $F(u) = F(-u)$, in the plasma rest frame, the dispersion equation (2.17) can be presented in the form

$$1 - n^2 + 2\frac{(1 - n^2\cos^2\theta_b))\omega_p^2}{\omega^2}\int_0^\infty \frac{\beta\,{\rm d}F/{\rm d}u}{1 - n^2\beta^2\cos^2\theta_b}{\rm d}u = 0, \tag{6.22}$$

from which one can see that it has two roots of n^2, which means that there are, as it were, two modes of oscillations. Adding the mode $n_1^2 = 1$, the total number of modes

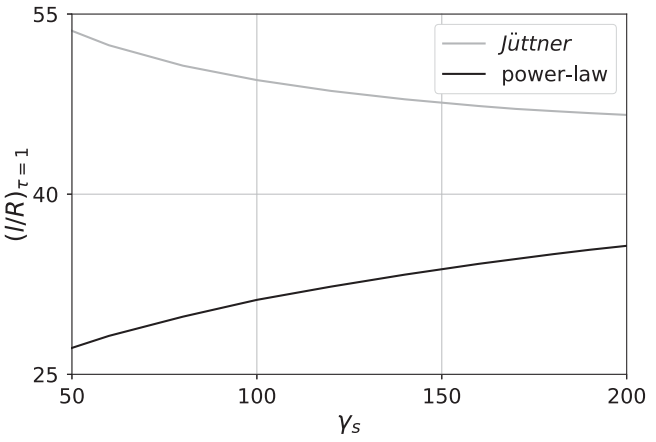

FIGURE 11. Comparison of levels $l = r_d$ at which the optical depth $\tau = 1$ (4.8) depending on parameter γ_s for both Jüttner ($\rho = 4$, γ_s) and power-law ($u_0 = \gamma_s/2$) distribution functions for the Alfvén mode $j = 4$.

is three. However, this is not so because $n = \pm(n^2)^{1/2}$, and the number of modes is six. The degeneracy is removed for the streaming distribution function, $F(u) \neq F(-u)$. Thus, the consideration of eigenmodes in the laboratory coordinate frame gives the same picture as the consideration in the rest frame.

7. Conclusion

It was shown that thermal kinetic effects do not affect so drastically the dispersion relations for all four waves propagating outwards in the pulsar magnetosphere. In particular, for the superluminal O-mode $j = 2$ the 'hydrodynamical' relation (2.10) yields a good enough expression for refractive index n_2. We intend to conduct a detailed analysis of thermal effects on the observed average profiles of radio pulsars in a separate paper.

As for the two subluminal modes $j = 3$ and $j = 4$, for them the kinetic effects result in more effective damping already at the angles $\theta_b \sim \theta^*$. In particular, it was shown that the attenuation of a plasma-Alfvén wave $j = 3$ substantially depends on the low-energy part of the spectrum of the outflowing particles: in the absence of a low-energy tail (see § 6), the attenuation occurs at the same distances from the star as for cold plasma. On the other hand, the presence of a high-energy power-law tail does not alter significantly the attenuation of the Alfvén wave $j = 4$ in comparison with the cold outflow. Remember that this is not so important because these modes cannot escape the pulsar magnetosphere as at a large distance from a neutron star they propagate along magnetic field lines.

As was already mentioned, a detailed analysis of astrophysical applications is beyond the scope of this paper. Nevertheless, it is worth discussing qualitatively the dependence of the above mentioned effects on the main parameters. Wherein, below we, again, consider only the regions which are close enough to the star surface (i.e. for which $A_p \gg 1$).

First of all, we note that the plasma effects considered above become most pronounced at low frequencies. As was already stressed, the ordinary O-mode $j = 2$ cannot propagate outward for $a_p > 1$, i.e. for small enough frequencies ω. According to (2.15), it takes place for $l < l_{\rm cr}$, where

$$l_{\rm cr} \sim 0.4R \left(\frac{P}{1\ {\rm s}}\right)^{-1/3} \left(\frac{B_0}{10^{12}\ {\rm G}}\right)^{1/3} \left(\frac{\lambda}{10^4}\right)^{1/3} \left(\frac{\gamma_s}{100}\right)^{-1} \left(\frac{\nu}{1\ {\rm GHz}}\right)^{-2/3}. \tag{7.1}$$

For example, for low-frequency array (known as LOFAR) frequencies $\nu \approx 30$ MHz we obtain $l_{\rm cr} \approx 20R$ for $P = 0.5$ s, $B_0 = 2 \times 10^{12}$ G and $\gamma_s = 50$. For this reason, Beskin *et al.* (1988) proposed this property to explain the low-frequency cut-off of the pulsar radio emission. On the other hand, it is clear that being emitted from larger distances, an ordinary wave $j = 2$ can freely escape the pulsar magnetosphere.

Next, let us briefly discuss the dependence on the Lorentz factor γ_s. If, according to Arendt & Eilek (2002), the averaged Lorentz factor is close to 10^3, then, according to (2.7) and (2.15), the value A_p becomes an order of magnitude greater, and, which is more important, the value a_p becomes three orders of magnitude smaller. As a result, the approximation under consideration turns out to be valid up to larger distances from the surface of the star, although the refraction effects themselves become much less pronounced.

On the other hand, if, in reality, $\gamma_s \approx 10$ (this may be due to the presence of a non-dipole magnetic field near the surface of the star, see, e.g. Arons (1993) for more detail), the situation can radically change. Indeed, as can be seen from relation (7.1), in this case, the ordinary O-mode can propagate from the star surface only starting from the heights more than $20R$, and at lower frequencies of the order of 100 MHz – only starting from the heights more than $100R$, which can lead to a direct contradiction with the observational data.

Further, one can see that the effect of multiplicity is not so significant as, according to (7.1), the dependence of the critical radius $l_{\rm cr}$ on λ does not turn out to be so sharp. On the other hand, for millisecond pulsars, it is parameter λ that can bring about a significant effect on the propagation effects. Indeed, for millisecond pulsars ($P \sim 2$–10 ms, $B_0 \sim 10^8$–10^9 G), the very value of the Goldreich–Julian number density $N_{\rm GJ}$ (2.4) does not change very noticeably. On the other hand, according to Timokhin & Harding (2015), the multiplicity λ is

$$\lambda \approx 5.4 \times 10^4 \left(\frac{R_c}{10^7\ {\rm cm}}\right)^{-3/7} \left(\frac{P}{1\ {\rm s}}\right)^{-1/7} \left(\frac{B_0}{10^{12}\ {\rm G}}\right)^{-6/7}, \tag{7.2}$$

where R_c is the curvature radius of the magnetic field lines, should be suppressed by several orders of magnitude. As a result, we obtain for the number density N_e (2.3) using standard evaluation of the curvature radius $R_c = (4/3)R/R_0$ for dipole magnetic field ($R_0 = R(\Omega R/c)^{1/2}$ is the polar cap radius):

$$N_e \approx 0.2 \times 10^8 \left(\frac{P}{1\ {\rm ms}}\right)^{-19/14} \left(\frac{B_0}{10^8\ {\rm G}}\right)^{-13/7} \left(\frac{l}{10R}\right)^{-3}. \tag{7.3}$$

As we see, the value of N_e (7.3) for millisecond pulsars is four orders of magnitude smaller than that of ordinary pulsars, see (2.3). Thus, according to (7.1), for millisecond pulsars, the region $A_p \gg 1$ considered above exists only for not very high heights $l < 10R$. Wherein, according to (7.1), the ordinary mode always propagates outside from the star surface. If the radiation is generated at larger distances from a neutron star, the refractive index (5.9) should be used for the O-mode.

In conclusion, let us comment on the three statements which were already mentioned above. First, it is necessary to stress that we confirmed that at zero angle θ_b in the laboratory (pulsar) reference frame, there are two branches of the same plasma wave propagating from a neutron star. But in the plasma rest frame both modes propagate inwards to the star surface, one of them ($j = 2$) being superluminal and the other ($j = 3$) subluminal. Second, it should be noted that our results do not contradict the conclusions obtained by

Rafat *et al.* (2019*b*). Indeed, as was shown in this paper, in the region of phase velocities corresponding to $\gamma_\phi < 100$ (i.e. precisely in the region $A_p > 1$), the results for the plasma modes $j = 2, 3$ are actually identical. In our opinion, the question on the number of waves can be considered closed. Finally, remember that in the theory of radio emission proposed by Beskin *et al.* (1988), the key role is played by the instability of the Alfvén mode $j = 4$ in the angle range $\theta_b < \theta^*$, which is connected with the curvature of magnetic field lines. As was shown above, the inclusion of thermal effects into consideration does not lead to strong attenuation of the Alfvén mode in this region. Thus, thermal effects do not violate significantly this key point of the theory.

Acknowledgements

We thank S. Philippov for useful discussions and all four anonymous reviewers for many insightful comments and suggestions.

Editor Roger Blandford thanks the referees for their advice in evaluating this article.

Declaration of interests

The authors report no conflict of interest.

Funding

This work was supported by the Russian Foundation for Basic Research (project no. 17-02-00788).

Appendix A. Damping of the plasma-Alfvén wave $j = 3$

In this appendix, we check whether our conclusion on the damping of the plasma-Alfvén wave $j = 3$ is correct in spite of the fact that the derivative $\mathrm{d}F/\mathrm{d}u$ is positive for resonance particles. For simplicity, we consider the waves propagating along the homogeneous magnetic field (in the direction of the x-axis).

First, remember that in our statement of the problem, in the laboratory (pulsar) reference frame only the wavevector k of the wave $j = 3$ has the imaginary part, the wave amplitude being constant at the radiating point $x = 0$ ($l = l_{\rm rad}$). In this system the wave amplitude E can be written as

$$E = E_0\,\mathrm{e}^{-\mathrm{i}\omega t+\mathrm{i}(\mathrm{Re}\,k)x-(\mathrm{Im}\,k)x}. \tag{A 1}$$

To show that the imaginary part $\mathrm{Im}\,k$ is really positive, let us consider a subluminal plasma wave propagating in the plasma rest frame along the magnetic field towards negative values x' (towards the star). In this frame, the coordinate of the radiating point $x = 0$ corresponds to $x' = -\beta_s ct'$. As was shown at the beginning of § 4, it is this wave that corresponds to the plasma-Alfvén wave $j = 3$ in the pulsar reference frame.

On the other hand, it is clear that in a plasma rest system this wave will decay as it propagates toward negative x'. Passing now in (A 1) to the variables (t', x') using the Lorentz transformation, we obtain, taking into account the invariance of the quantity $kx - \omega t$,

$$E = E_0\,\mathrm{e}^{-\mathrm{i}\omega' t'+\mathrm{i}(\mathrm{Re}\,k')x'-(\mathrm{Im}\,k)(x'+c\beta_s t')}. \tag{A 2}$$

As expected, the wave amplitude remains constant at the radiating point $x' = -c\beta_s t'$.

Further, since in the laboratory (pulsar) reference frame this wave propagates outwards from a neutron star, in the plasma rest frame its velocity should be less than the relative velocity of the reference systems ($|\beta| < \beta_s$). As a result, on the wave trajectory $x' = -c\beta t'$,

the amplitude (A 2) has the form

$$E = E_0\, \mathrm{e}^{-\mathrm{i}\omega' t' + \mathrm{i}(\mathrm{Re}\, k')x' - (\mathrm{Im}\, k)(\beta_s - \beta)ct')}. \tag{A 3}$$

Since this wave must attenuate with increasing t', we conclude that $\mathrm{Im}\, k > 0$, which corresponds to damping of the plasma-Alfvén wave in the pulsar reference frame. Thus, here we are also dealing with convective stability/instability, which depends on the reference frame (Landau & Lifshits 1981).

REFERENCES

Andrianov, A. S. & Beskin, V. S. 2010 Limiting polarization effect - a key link in investigating the mean profiles of radio pulsars. *Astron. Lett.* **36**, 248–259.

Arendt, P. N. & Eilek, J. A. 2002 Pair creation in the pulsar magnetosphere. *Astrophys. J.* **581**, 451–469.

Arons, J. 1993 Magnetic field topology in pulsars. *Astrophys. J.* **408**, 160–166.

Asseo, E., Pellat, R. & Sol, H. 1983 Radiative or two-stream instability as a source for pulsar radio emission. *Astrophys. J.* **266**, 201–214.

Asseo, E., Pelletier, G. & Sol, H. 1990 A non-linear radio pulsar emission mechanism. *Mon. Not. R. Astron. Soc.* **247**, 529–548.

Barnard, J. J. & Arons, J. 1986 Wave propagation in pulsar magnetospheres - refraction of rays in the open flux zone. *Astrophys. J.* **302**, 138–162.

Benford, G. & Buschauer, R. 1977 Coherent pulsar radio radiation by antenna mechanisms: general theory. *Mon. Not. R. Astron. Soc.* **179**, 189–207.

Beskin, V. S., Gurevich, A. V. & Istomin, Ya. N. 1988 Theory of the radio emission of pulsars. *Astrophys. Space Sci.* **146**, 205–281.

Beskin, V., Gurevich, A. & Istomin, Y. 1993 *Physics of the Pulsar Magnetosphere*. Cambridge University Press.

Beskin, V. S. & Philippov, A. A. 2012 On the mean profiles of radio pulsars - I. Theory of propagation effects. *Mon. Not. R. Astron. Soc.* **425**, 814–840. arXiv:1107.3775.

Blandford, R. D. 1975 Amplification of radiation by relativistic particles in a strong magnetic field. *Mon. Not. R. Astron. Soc.* **179**, 551–557.

Blandford, R. D. & Scharlemann, E. T. 1976 On the scattering and absorption of electromagnetic radiation within pulsar magnetospheres. *Mon. Not. R. Astron. Soc.* **174**, 59–85.

Blaskiewicz, M., Cordes, J. M. & Wasserman, I. 1991 A relativistic model of pulsar polarization. *Astrophys. J.* **370**, 643–669.

Daugherty, J. K. & Harding, A. K. 1982 Electromagnetic cascades in pulsars. *Astrophys. J.* **252**, 337–347.

Dyks, J. 2008 Altitude-dependent polarization in radio pulsars. *Mon. Not. R. Astron. Soc.* **391**, 859–868. arXiv:0806.0554.

Gedalin, M., Gruman, E. & Melrose, D. B. 1999 Mechanism of pulsar radio emission. *Mon. Not. R. Astron. Soc.* **337**, 422–430.

Ginzburg, V. L. & Zheleznyakov, V. V. 1975 On the pulsar emission mechanisms. *Annu. Rev. Astron. Astrophys.* **13**, 511–535.

Goldreich, P. & Keeley, D. A. 1971 Coherent synchrotron radiation. *J. Plasma Phys.* **170**, 463–478.

Gurevich, A. V. & Istomin, Ya. N. 1985 Generation of electron-positron plasma in a pulsar's magnetosphere. *Sov. Phys. JETP* **62**, 1–11.

Hakobyan, H. L., Beskin, V. S. & Philippov, A. A. 2017 On the mean profiles of radio pulsars II: reconstruction of complex pulsar light-curves and other new propagation effects. *Mon. Not. R. Astron. Soc.* **469**, 2704–2719.

Han, J. L., Manchester, R. N., Xu, R. X. & Qiao, G. J. 1998 Circular polarization in pulsar integrated profiles. *Mon. Not. R. Astron. Soc.* **300**, 373–387. arXiv:astro-ph/9806021.

Hardee, P. E. & Rose, W. K. 1978 Wave production in an ultrarelativistic electron-positron plasma. *Astrophys. J.* **219**, 274–287.

KAZBEGI, A. Z., MACHABELI, G. Z. & MELIKIDZE, G. I. 1991 On the circular polarization in pulsar emission. *Mon. Not. R. Astron. Soc*. **253**, 377–387.

LANDAU, L. D. & LIFSHITS, E. M. 1981 *Physical Kinetics*. Pergamon.

LARROCHE, O. & PELLAT, R. 1987 Curvature instability of relativistic particle beams. *Phys. Rev. Lett*. **59**, 1104–1107.

LOMINADZE, J. G., MACHABELI, G. Z. & USOV, V. V. 1983 Theory of np:0532 pulsar radiation and the nature of the activity of the crab nebula. *Astrophys. Space Sci*. **90**, 19–43.

LOMINADZE, D. G. & MIKHAILOVSKII, A. B. 1979 Longitudinal waves and the beam instability in a relativistic plasma. *Sov. Phys. JETP* **49**, 483–489.

LOMINADZE, D. G., MIKHAILOVSKII, A. B. & SAGDEEV, R. Z. 1979 Langmuir turbulence of a relativistic plasma in a strong magnetic field. *Sov. Phys. JETP* **50**, 927–932.

LORIMER, D. R. & KRAMER, M. 2012 *Handbook of Pulsar Astronomy*. Cambridge University Press.

LYNE, A. & GRAHAM-SMITH, F. 2012 *Pulsar Astronomy*. Cambridge University Press.

LYUBARSKY, Y. 2008 Pulsar emission mechanisms. In *40 Years of Pulsars: Millisecond Pulsars, Magnetars and More* (ed. A. Cumming C.G. Bassa, Z. Wang & V.M. Kaspi), AIP Conference Proceedings, American Institute of Physics, vol. 983, pp. 29–37.

LYUBARSKII, Y. E. & PETROVA, S. A. 1998 Refraction of radio waves in pulsar magnetospheres. *Astron. Astrophys*. **333**, 181–187.

LYUBARSKII, Y. E. & PETROVA, S. A. 2000 Propagation effects in pulsar magnetospheres. *Astron. Astrophys*. **355**, 1168–1180.

LYUTIKOV, M. 1999 Beam instabilities in a magnetized pair plasma. *J. Plasma Phys*. **62**, 65–86.

LYUTIKOV, M., BLANDFORD, R. & MACHABELI, G. 1999 On the nature of pulsar radio emission. *Mon. Not. R. Astron. Soc*. **305**, 338–352.

MACIESIAK, K., GIL, J. & MELIKIDZE, G. 2012 On the pulse-width statistics in radio pulsars III. Importance of the conal profile components. *Mon. Not. R. Astron. Soc*. **424** (3), 1762–1773.

MANCHESTER, R. & TAYLOR, J. 1977 *Pulsars*. Freeman.

MEDIN, Z. & LAI, D. 2010 Pair cascades in the magnetospheres of strongly magnetized neutron stars. *Mon. Not. R. Astron. Soc*. **406**, 1379–1404.

MELROSE, D. B. & GEDALIN, M. E. 1999 Relativistic plasma emission and pulsar radio emission: a critique. *Astrophys. J*. **521**, 351–361.

MELROSE, D. B. & RAFAT, M. Z. 2017 Pulsar radio emission mechanism: why no consensus? *J. Phys.: Conf. Ser*. **932**, 012011.

MELROSE, D. B., RAFAT, M. Z. & MASTRANO, A. 2020 Pulsar radio emission mechanisms: a critique. *Mon. Not. R. Astron. Soc*. **500**, 4530–4548.

MESTEL, L. 1999 *Pulsars*. Clarendon.

MICHEL, F. C. 1991 *Theory of Pulsar Magnetospheres*. University of Chicago Press.

MITRA, D. 2017 Nature of coherent radio emission from pulsars. *J. Astron. Astrophys*. **38**, 52.

PETROVA, S. A. 2001 The effect of magnetospheric refraction on the morphology of pulsar profiles. *Mon. Not. R. Astron. Soc*. **360**, 592–602.

PHILIPPOV, A., TIMOKHIN, A. & SPITKOVSKY, A. 2020 Origin of pulsar radio emission. *Phys. Rev. Lett*. **24**, 245101.

PHILIPPOV, A., UZDENSKY, D. A., SPITKOVSKY, A. & CERUTTI, B. 2019 Pulsar radio emission mechanism: radio nanoshots as a low-frequency afterglow of relativistic magnetic reconnection. *Astrophys. J*. **876**, 6–12.

RAFAT, M. Z., MELROSE, D. B. & MASTRANO, A. 2019*a* Wave dispersion in pulsar plasma: 1. Plasma rest frame. *J. Plasma Phys*. **85**, 905850305.

RAFAT, M. Z., MELROSE, D. B. & MASTRANO, A. 2019*b* Wave dispersion in pulsar plasma: 2. Pulsar frame. *J. Plasma Phys*. **85**, 905850311.

RANKIN, J. M. 1990 Toward an empirical theory of pulsar emission. IV - geometry of the core emission region. *Astrophys. J*. **352**, 247–257.

SUVOROV, E. V. & CHUGUNOV, I. V. 1975 Electromagnetic waves in a relativistic plasma with a strong magnetic field. *Astrophysics* **11**, 203–222.

TIMOKHIN, A. N. 2010 A model for nulling and mode changing in pulsars. *Mon. Not. R. Astron. Soc*. **408**, L41–L45.

TIMOKHIN, A. N. & HARDING, A. K. 2015 On the polar cap cascade pair multiplicity of young pulsars. *Astrophys. J.* **810**, 144. arXiv:1504.02194.

URSOV, V. N. & USOV, V. V. 1988 Plasma flow nonstationarity in pulsar magnetospheres and two-stream instability. *Astrophys. Space Sci.* **140**, 325–336.

USOV, V. V. 1987 On two-stream instability in pulsar magnetospheres. *Astrophys. J.* **320**, 333–335.

USOV, V. V. 2006 Radio emission theories of pulsars. In *On the Present and Future of Pulsar Astronomy* (ed. J. Gil, W. Becker & B. Rudak), Highlights of Astronomy, Cambridge University Press, vol. 14, p. 4.

VOLOKITIN, A. S., KRASNOSELSKH, V. V. & MACHABELI, G. Z. 1985 Waves in the relativistic electron-positron plasma of a pulsar. *Sov. J. Plasma Phys.* **11**, 310–314.

WANG, C., LAI, D. & HAN, J. 2010 Polarization changes of pulsars due to wave propagation through magnetospheres. *Mon. Not. R. Astron. Soc.* **403**, 569–588.

WANG, P. F., WANG, C. & HAN, J. L. 2014 Polarized curvature radiation in pulsar magnetosphere. *Mon. Not. R. Astron. Soc.* **441**, 1943–1953.

WANG, P. F., WANG, C. & HAN, J. L. 2015 On the frequency dependence of pulsar linear polarization. *Mon. Not. R. Astron. Soc.* **448**, 771–780.

WEATHERALL, J. C. 1994 Streaming instability in relativistically hot pulsar magnetospheres. *Astrophys. J.* **428**, 261–266.

YUEN, R. & MELROSE, D. B. 2014 Visibility of pulsar emission: motion of the visible point. *Publ. Astron. Soc. Aust.* **31**, e039.

ZHELEZNYAKOV, V. V. 1970 *Radio Emission of the Sun and Planets*. Pergamon.